

Correlations in a Many-Body Calculation of ^{11}Li

C. R. Chinn

Department of Physics and Astronomy

Vanderbilt University, Nashville, TN 37235

J. Dechargé and J.-F. Berger

Service de Physique et Techniques Nucléaires

Centre d'Etudes de Bruyères-le-Châtel

B.P. No. 12, 91680 Bruyères-le-Châtel, FRANCE

Abstract

A many-body calculation of ^{11}Li is presented where the only input is the well-tested, finite-range *DIS* effective interaction of *Gogny*. Pairing correlations are included in a constrained Hartree-Fock-Bogolyubov calculation, while long-range collective correlations are introduced using a GCM derived calculation. Correlations are found to play an important role in describing ^{11}Li . A substantive underlying ^9Li core of ^{11}Li is found, which has a different density profile than a free ^9Li nucleus. This may have significant implications in the use of a three-body framework in studies of

^{11}Li .

I. INTRODUCTION

With the recent advent of secondary beam facilities there has been a large research interest in nuclei near the drip lines. These exotic nuclei offer opportunities to study many-body effects under unusual conditions. An example of such can be related to the nucleon-nucleon [N-N] interaction. While the free N-N interaction appears to be well understood, the role of the N-N interaction in microscopic nuclear structure is far from being clear. (One example where one would think that the role of the N-N interaction should be clear, but is not is in the ${}^3\text{H}$ problem.) Because nuclei near the drip line have weak binding energies and hence large density distributions, the N-N interaction can now be studied in regions of low nuclear density.

The free neutron-neutron [n-n] interaction is attractive, but the di-neutron system is unbound. Migdal and Watson postulated the possibility that a di-neutron may become bound if placed within the field of a nucleus. ${}^{11}\text{Li}$ among others appears to be such a system, since both ${}^{11}\text{Li}$ and ${}^9\text{Li}$ are bound while ${}^{10}\text{Li}$ is not. Hence, with this in mind, recent interest in ${}^{11}\text{Li}$ has been strongly addressed within a three-body framework [1–6], where ${}^{11}\text{Li}$ is represented as two neutrons surrounding an inert ${}^9\text{Li}$ core. For a recent review of such work, please see Ref. [1].

The assumption that ${}^{11}\text{Li}$ can be realistically represented as a three-body system needs to be investigated. While present experimental evidence indicates that this assumption may be valid [7,8], one would like to test this hypothesis within a many-body theoretical investigation. Difficulties that may arise with the three-body framework include: 1.) treatment

of the Pauli exclusion principle can only be performed approximately, and 2.) correlations with the ${}^9\text{Li}$ core are ignored.

The most straightforward way to study ${}^{11}\text{Li}$ in an A -body framework is to use a single particle model, but this was shown for this nucleus [9] to give an inadequate description. Therefore, for a proper A -body calculation a correlated description beyond a single particle model is required. By renormalizing the mean field potential several groups [9–11] found that the experimental two neutron separation energy and the *rms* radius of ${}^{11}\text{Li}$ could be reproduced, thus indicating the possible existence of correlations among the outer single particle states. An attempt to model correlations in a shell model description [12] resulted in small effects, but as will be shown later in this paper the adopted shell model space used in this study is clearly too small.

In this paper we introduce long-range correlations by using a Generator Coordinate Method [GCM] type formalism. The nuclear ground state [GS] is represented as a superposition of HFB nuclear states, which are obtained by constraining on different values of the $\langle r^2 \rangle$ collective variable. The reason for choosing this particular GCM variable can be understood in the following way: correlations in the ${}^{11}\text{Li}$ GS are expected to occur because the loosely bound outer neutrons can occupy a large number of nearly degenerate Rydberg-type orbits having a broad range of radial extensions. One expects that a constraint imposing different values of the total *rms* radius will act essentially on the outer neutrons radial distributions and therefore will be able to generate the kind of configurations present in the nuclear GS. Therefore, as is usual in GCM calculations, initially, a series of constrained HFB microscopic mean field calculations is performed. In a second step the coefficients of the

GCM configuration mixing are computed by solving the coupled equations resulting from the application of a variation principle to the total nucleus binding energy. In the present work, this is accomplished in an approximate fashion by reducing the usual Hill-Wheeler equations to a collective Schrödinger equation of the Bohr type. Note that this calculation includes pairing correlations as well as long-range collective degrees of freedom as derived from the effective N-N interaction. Also, the Pauli principle is strictly obeyed through the use of fully antisymmetrized single particle wave functions.

The only input into this consistent A -body calculation is the well-tested *DIS Gogny* force. This interaction is a density-dependent phenomenological parametrization of the N-N interaction inside the nuclear medium which includes a spin-orbit term, and is finite-ranged. The parameters of the interaction have been fixed by matching the bulk properties of nuclear matter and of a few finite nuclei, including pairing correlation strengths. This *DIS* force has been tested in a variety of applications with excellent results [13,14]. It must be noted that this force gives a very good description not only of medium and heavy nuclei, but also of very light nuclei. For instance it describes correctly the binding energy and radius of the alpha particle. In addition the finite range, density-independent part of the force has been set-up in order to roughly simulate a free N-N interaction in the sense that it gives the correct N-N scattering lengths. These properties are important in the present context which deals with a three-proton system where almost free neutron-neutron interactions are expected to play a crucial role.

With this collective model a qualitative study of correlations in ^{11}Li is presented. In particular the role of the ^9Li core is explored, especially its relation to a free ^9Li nucleus.

The validity of the three-body hypothesis is investigated using a collective A -body model.

In Section II the mean field constrained and unconstrained HFB calculation is described and the results presented. Long-range correlations using a simplification of the GCM is described in Section III along with the results and analysis, followed by a conclusion.

II. CONSTRAINED HFB CALCULATION

The constrained HFB A -body calculation is performed using a nineteen shell axially-symmetric harmonic oscillator [HO] basis. In performing tests of the convergence of the basis, it was found that a nineteen shell basis is required due to the large extension of the neutron matter distribution from the center of the nucleus in coordinate space, and to the inadequate asymptotic behavior of HO states in r space. The use of a multi-oscillator basis, *i.e.* of a basis composed of several sets of concentric HO states associated with different lengths is also used in the HFB calculation. This kind of basis allows one to extend to larger distances the radial description of nucleon orbits. However, in this case only spherically symmetric nuclear distributions could be described. Time-reversal symmetry is assumed, so the protons are described by blocking with equal weights the two $j_z^\pi = \pm 3/2^-$ axial quasi-particle orbitals, thus matching the known ground state spin of both ^{11}Li and ^9Li .

For a study of a small nucleus such as ^{11}Li , it would be expected that a mean field description would not be the most appropriate choice. In this case we wish to address certain many-body questions and to test assumptions about the many-body nature of the problem. With this in mind as a first step, a mean field calculation using HFB should be able to

address some of these qualitative concerns.

As explained in the Introduction, the ^{11}Li nucleus is expected to be very soft against changes in the density distribution *rms*. For this reason a constrained HFB calculation was performed, where the constraint variable used corresponds to the mean value of $\langle r^2 \rangle$:

$$q = \int dr r^2 \rho(r) , \text{ where } \rho(r) = \int d\Omega \rho(\vec{r}) , \quad (1)$$

$$\langle r_{rms} \rangle = \sqrt{q}$$

When the constraint is switched off, one gets the mean-field representation of the ^{11}Li GS. The total *rms* matter radius obtained in this way is about 2.80 fm, matching the results of several other groups [12,9]. The separate proton and neutron *rms* radii are found to be 2.30 and 2.97 fm, respectively. For a similar HFB calculation of the ^9Li GS the *rms* radii are found to be 2.47, 2.24, and 2.58 fm for the total, proton and neutron distributions, respectively. The *rms* radii for the protons in ^9Li and ^{11}Li differ only by a small amount in these mean-field calculations, resulting from the effects of the force between the neutrons and the protons. However, when correlations are introduced in ^{11}Li , if there is an uncorrelated ^9Li core in ^{11}Li , it may well differ from the free ^9Li GS. It remains to be seen though how large this difference may be.

In Fig. 1 the results of the constrained ^{11}Li calculation are shown as a function of the constraint variable, q . A similar spherical ^9Li calculation is also shown. As q is increased, the ^{11}Li curve is much softer than ^9Li in the sense that the slope is much less steep. One then expects ^{11}Li to include significantly more configuration mixing than ^9Li . Such a mixing

has been included and will be discussed in detail later.

The *rms* radii for the neutron and proton distributions are shown in Fig. 2a for the constrained HFB results as a function of $\langle r_{rms} \rangle_{total} = \sqrt{q}$. As expected (see the Introduction) the proton *rms* is unaffected by the constraint, while the neutron $\langle r_{rms} \rangle_n$ varies linearly. In other words, the curve confirms that the potential between the protons and outer neutrons is not strong enough to prevent the two distributions from decoupling.

The independent nature of the proton and neutron sectors is also evident in the pairing energy shown in Fig. 2b. The protons consistently have zero pairing as a function of q . The neutrons have strong pairing for $q > 3$ fm indicating the onset of a significantly high neutron level density at the Fermi surface.

Since the protons do not exhibit pairing there must be a sizeable gap at the Fermi surface. This is shown in Fig. 3a, where the protons occupying the $1s_{1/2}$ and $1p_{3/2}$ states. There is a gap of about 6 MeV between the $1p_{3/2}$ level and the higher single particle levels and this gap remains for all q considered. The relative energies of the occupied levels do not change significantly as a function of q , confirming the negligible influence of the constraint on the proton mean-field. Note that, since the $1p_{3/2}$ level does not shift a great deal, the blocking approximation used here to account for the odd number of protons should be reasonable.

In Fig. 3b the corresponding neutron single particle levels are shown. The lowest six neutrons are almost completely contained in the $1s_{1/2}$ and $1p_{3/2}$ orbitals. Due to pairing correlations the last two neutrons are dispersed throughout the higher levels. There is almost

no gap between the $1p_{1/2}$ level and the higher levels, and for large q these levels cross. The levels higher than $2d_{3/2}$ are not shown. The level density at the Fermi surface is very high, indicating that configuration mixing, *i.e.* the existence of correlations is widespread.

This result is an indication that the model space required to describe the ^{11}Li GS in an extended shell model calculation is much larger than generally assumed [12]. According to the present calculation levels above the f shell surely contribute to the GS description.

In Fig. 3b it is clear that there is a large gap between the six inner neutrons, which represent a ^9Li core, and the outer two valence neutrons. The calculated occupation probabilities for the core neutrons are almost always between 1.00 and 0.99 with a minimum of $\gtrsim 0.987$. This is true for all q considered. Because of these features, a ^9Li core wave function can be projected out by taking the constrained HFB ^{11}Li solutions and explicitly setting the first six neutron levels to have one occupation probability and the other neutron levels to be empty. As evidenced by the fact that the core neutron probabilities are not exactly one, this is an approximate procedure, but clearly, because of the large energy gap, this should be a very reasonable and accurate representation.

In Fig. 4 the neutron density profiles are shown for the unconstrained HFB calculations of ^9Li and ^{11}Li , and for the ^9Li core projected from ^{11}Li as explained above. At the center of the nucleus the free ^9Li neutron density is sizeably larger than the ^9Li core neutron density, and accordingly, the ^9Li core extends somewhat farther. More precisely, the central neutron density of ^9Li (short-dashed curve) is about 15% larger than that of the ^9Li core (long dashed curve). A similar difference was found for the protons. This is more easily seen when the

tail is expanded in a logarithmic plot. The the ^{11}Li core neutrons density doesn't fall off as rapidly beyond $r = 7$ fm. Already one can see evidence for the beginning of a halo-like structure.

III. CALCULATION INCLUDING CONFIGURATION MIXING

From the evidence shown in the previous two sections it is clear that a pure single particle model is inadequate to describe ^{11}Li . To provide a more sophisticated representation, a correlated ground state wave function is constructed as a superposition of the HFB nuclear states in the following GCM form:

$$|\chi_o\rangle = \int dq f_o(q) |\phi_q\rangle , \quad (2)$$

where $|\phi_q\rangle$ is a product of HFB quasiparticle states for deformation q , $f_o(q)$ is a weight function, and q is the constraint variable. In the GCM formalism a hamiltonian kernel is constructed with the GCM wave function. By applying the variational principle, an equation is derived from which the weight functions can be calculated. A Gaussian overlap approximation [GOA], where the overlap between any two HFB states is approximated by a Gaussian in the collective variable [15], is applied to simplify these equations, deriving a Bohr Hamiltonian expression. The solution of the Bohr Hamiltonian equation gives the weight function, $f_o(q)$. These techniques have been thoroughly tested in many instances [16]. It may be that the GOA is not as accurate for smaller nuclei as in previous experience, but for the investigative study being performed here, this should be more than adequate.

The resulting ground state collective wave function, $f_o(q)$, has a corresponding total binding energy. To properly calculate the two neutron separation energy it is necessary to perform a similar collective calculation for the free ${}^9\text{Li}$ case and then to take the difference in the total collective binding energies. As shown in Ref. [9] the energies calculated from the single particle HFB model are inadequate and it is necessary to include more sophisticated degrees of freedom.

The ground state correlated density is calculated from (2) in the following fashion:

$$\rho_{GS}(r) = \int dq' \int dq f_o(q') \langle \phi_{q'} | \hat{\rho}_o(r) | \phi_q \rangle f_o(q), \quad (3)$$

where $\hat{\rho}_o(r)$ is the radial density operator obtained after angle averaging.

In Fig. 5 the proton density profile is shown from the unconstrained HFB calculation of ${}^9\text{Li}$ and ${}^{11}\text{Li}$ along with the GCM-type collective result for ${}^{11}\text{Li}$. As is apparent here the ${}^9\text{Li}$ and ${}^{11}\text{Li}$ proton profiles are not equivalent, implying differences between the free ${}^9\text{Li}$ nucleus and the ${}^9\text{Li}$ core of ${}^{11}\text{Li}$. The correlated ${}^{11}\text{Li}$ proton density is very similar to the uncorrelated ${}^{11}\text{Li}$ result, which should not be surprising in light of the unchanging single particle spectrum in Fig. 3a. For the protons the correlations have little effect upon the density distributions both near the central part and along the tail. It appears clear that there are few correlations in the ${}^{11}\text{Li}$ proton sector.

The various neutron distributions are shown in Fig. 6. As in the unconstrained HFB case an approximate representation of the ${}^9\text{Li}$ core can be projected out from the ${}^{11}\text{Li}$ calculation including configuration mixing. This is performed by setting the neutron occupation probabilities in the constrained HFB solutions to be either one or zero and then using these

density matrices with the weight function, $f_o(q)$, obtained in the collective ^{11}Li calculation. As for the proton case the influence of correlations on the ^9Li core appears quite small. The collective long-range correlations represented by the GCM therefore have little effect on the ^9Li core as a whole.

This influence is much bigger on the full ^{11}Li neutron distribution, that is when one includes the two extra neutrons. The surface of the neutron distribution of ^{11}Li is at about ~ 2.5 fm, which is much further extended than the surface of the proton distribution at ~ 1.8 fm. Correlations slightly reduce this difference. Subtracting the ^9Li core neutron distribution from the ^{11}Li neutrons gives the structure of the two valence neutrons. The two neutrons have zero density at the origin due to the Pauli blocking from the core and extend in a halo-like structure. At the surface the collective valence structure causes the collective calculation to have a different neutron density profile than the unconstrained HFB neutrons.

This is most easily seen on the logarithmic plot in the lower part of Fig. 6 : the HFB and GCM GS ^{11}Li neutron densities strongly differ beyond $q = 6$ fm. At this point it must be emphasized that an unphysical ledge appears in the GCM densities beyond $q = 7 - 8$ fm. This ledge is small in amplitude, but it affects greatly the calculated *rms* radius since it extends very far out. The origin of this ledge can be traced back to the structure of the HFB constrained solutions included in the configuration mixing. In Fig. 7 the neutron densities obtained in constrained HFB calculations using the nineteen shell basis at $q = 3.4$ fm and $q = 4$ fm are shown. Also shown are the same results using a multi-oscillator spherical HFB basis. This particular multi-oscillator basis uses three concentric sets of eight shell bases with three different oscillator lengths. This basis corresponds to a very large single oscillator

basis (≈ 60 shells). Clearly, a ledge appears in the HFB densities which depends on the basis. With the large multi-oscillator basis the ledge appears two orders of magnitude smaller and at larger r . This ledge is a result of the constraint on $\langle r^2 \rangle$, that tends to push up the density at large r , but then is restricted by the local nature of the harmonic oscillator bases. One in fact observes the parabolic fall of the densities in the 19 shell HO basis, characteristic of the HO asymptotic behavior at large r . A similar parabolic fall of the multi-oscillator densities is also observed at very large r (30 fm). Both the property of r^2 to be unbounded and the use of a restricted HO space may be responsible for this phenomenon

Since there clearly exists a great deal of configuration mixing in ^{11}Li due to the radial extension of outer neutrons, one would also like to be able to extract a reasonable asymptotic tail for the GS wave function. This is necessary to get a reasonable estimate of the GS neutron *rms* radius. The single particle wave functions should asymptotically be proportional to:

$$\sim \frac{e^{-\kappa r}}{r}, \quad \kappa = \sqrt{\frac{-2\mu E}{\hbar^2}}. \quad (4)$$

where E is the single particle energy. For large but finite r a polynomial in $1/r$ should be included. Therefore, one expects the HFB neutron density to behave for large r , $r > r_o$ say, as:

$$\langle q | \rho(r) | q \rangle = \rho_o(q) \frac{e^{-2\alpha_q r}}{r^2} \left[1 + \frac{b_q}{r} + \frac{c_q}{r^2} \right]^2, \quad (5)$$

This form has been used to extrapolate the densities obtained in the multi-oscillator basis for values of r beyond the values where the unphysical ledge begins. The parameters α_q , b_q

and c_q were obtained by using a χ^2 fitting routine. $\rho_o(q)$ was chosen to match the small r density profile at r_o , where the tail was attached to the single oscillator calculation, typically at about 7 fm. The off-diagonal terms in the correlated densities (3) could then be computed from:

$$\langle q' | \rho(r) | q \rangle \propto \frac{e^{-(\alpha_{q'} + \alpha_q)r}}{r^2} \left[1 + \frac{b_{q'}}{r} + \frac{c_{q'}}{r^2} \right] \left[1 + \frac{b_q}{r} + \frac{c_q}{r^2} \right]. \quad (6)$$

There is a great deal of freedom in the choice of the tail parameters and hence we were able to obtain various different parameter sets, depending on how we chose to fix things. The α_q parameters were set to be between $0.10 \rightarrow 0.15$, which corresponds to energies of about $-0.21 \rightarrow -0.47$ MeV.

With these fitted tails Fig. 8 is obtained. Different sets of fitted tail parameters are labeled by a, b, c, d, e. They give slightly but not very different values for the extrapolated density above 10^{-6} . Note that here the tails extend further out than for the unconstrained HFB case.

Let us now turn to result concerning *rms* radii. In Table I the *rms* radii for the various densities of figs. 4, 5 and 6 are shown. The correlations change the calculated *rms* radii for the ${}^9\text{Li}$ core by only about 2%, which is consistent with the previous observation that correlations have a negligible effect upon the core. In this change the tail correction made above plays almost no role. As to the differences in the *rms* radii between the ${}^9\text{Li}$ nucleus and the values calculated for the ${}^9\text{Li}$ core, they are about 5% for both the protons and the neutrons. This effect upon the *rms* radius appears to be small, but the comparison of the density distributions made in the previous section yields a more pronounced difference. One may say

that the ${}^9\text{Li}$ system is slightly inflated when two extra neutrons are added. This comparison assumes that the ${}^9\text{Li}$ nucleus ground state wave function is not significantly influenced by correlations, which certainly is reasonable in view of the insensitivity of correlations on the ${}^9\text{Li}$ core. Again, the comparisons made for the nine-nucleon systems don't depend on the tail correction introduced previously. One may conclude that in this many-body calculation of ${}^{11}\text{Li}$ there appears to exist a substantive ${}^9\text{Li}$ core which notably differs from a free ${}^9\text{Li}$ nucleus. One expects that these differences may have a nonnegligible effect upon the mean field felt by the two outer neutrons.

Going to the full ${}^{11}\text{Li}$ *rms* radii, the value listed in Table I with correlations included, but without tail correction (3.42 fm), clearly is overestimated. In Table II the *rms* radii obtained without and with the various parametrized tail corrections are listed. The largest $\langle r_{rms} \rangle_{tot}$ using a fitted tail is case *a* with 2.88 fm. In the calculations performed here, the increase in *rms* radii due to correlations is between $\sim 0.04 \rightarrow 0.08$ fm with realistic tails. This result is somewhat disappointing in view of the the amount of complexity put into the GS wave-functions. The total and neutron *rms* radii, although not so far from consistent with the experimental error bars, appear 0.2 fm smaller than the nominal experimentally extracted values.

At this point, one may note that the present radius results probably represent lowest values. In fact, when using the multi-oscillator basis the resulting potential energy surface appears somewhat flatter than the nineteen shell basis shown in Fig. 1. This indicates that a fully realistic calculation where density tails would be correctly described, would also yield a much softer collective potential and therefore a stronger configuration mixing.

Hence effects of correlations larger than those derived here, especially with respect to the *rms* radius predictions, would certainly be found.

Finally let us mention that, since the present ^{11}Li calculations were performed assuming axial symmetry, we were able to calculate the electric quadrupole moments, both in the HFB and correlated calculations. It should be realized that since the proton sector was calculated with a blocking approximation, the ground state spin of the nucleus has been artificially set. In Table III the calculated axial quadrupole moments are displayed for ^{11}Li and ^9Li . Since the proton sector is not greatly affected by the correlations, the HFB and correlated GCM calculations give approximately the same charge quadrupole moment. Both of these results give remarkable agreement with the experimental result. The free ^9Li HFB result is also shown, where here the agreement is not nearly as close.

IV. CONCLUSIONS

A microscopic many-body calculation of ^{11}Li is presented with correlations. Pairing correlations are included in a constrained HFB calculation, while important long-range correlations are incorporated using a GCM type formalism. The sole input into the calculation is the well-tested, finite-range *DIS* effective interaction.

It was found that long-range correlations play an important role in the description of ^{11}Li . A distinct ^9Li core was found which remained uncoupled to both pairing and long-range correlations. The correlations were restricted almost exclusively to the sector occupied by the two valence neutrons. This substantive core appears to support the use of a three-

body framework to study this nucleus, although several factors must be considered. The Pauli principle acting between the ${}^9\text{Li}$ core neutrons and the two valence neutrons must be taken into account as seen in Fig. 6. Also, the ${}^9\text{Li}$ core found here appears to have a significantly different density profile than a free ${}^9\text{Li}$ nucleus. It may be necessary for three-body calculations to take into account the different density shape of the ${}^9\text{Li}$ core if more accurate calculations of this type are desired than those presently in existence.

Difficulties in this many-body treatment of ${}^{11}\text{Li}$ were encountered due to the use of naturally localized harmonic oscillator bases. Even with the use of an extended multi-oscillators dependences upon the basis were found. For a more complete and accurate calculation it would be necessary to use a better basis representation, which can accomodate a nucleus with a large extended tail. For example a collocation Basis spline basis in a very large box would probably work well.

Acknowledgements: Appreciation is extended to J. Luis Egidio for bringing our attention to this problem and to M. Girod, V. Khodel and R. M. Thaler for valuable discussions. One of the authors (CRC) would like to acknowledge the gracious hospitality of the Service de Physique et Techniques Nucléaires at Bruyères-le-Châtel where this research was performed.

REFERENCES

- [1] M. V. Zhukov, B. V. Danilin, D. V. Fedorov, J. M. Bang, I. J. Thompson and J. S. Vaagen, Phys. Rep. **231** (1993), 151.
- [2] J. M. Bang, I. J. Thompson, M. V. Zhukov, B. V. Danilin, D. V. Fedorov and J. S. Vaagen, Niels Bohr Institute preprint # NBI-91-31; J. M. Bang and I. J. Thompson, Phys. Lett. **B 279** (1992) 201.
- [3] Y. Tosaka and Y. Suzuki, Nucl. Phys. **A512** (1990) 46.
- [4] A. S. Jensen and K. Riisager, Nucl. Phys. **A537** (1992) 45.
- [5] L. Johannsen, A. S. Jensen and P. G. Hansen, Phys. Lett. **B 244** (1990) 357. P. G. Hansen and B. Jonson, Europhys. Lett. **4** (1987) 409.
- [6] A. C. Hayes, Phys. Lett. **B 254** (1991) 15.
- [7] I. Tanihata, T. Kobayashi, O. Yamakawa, S. Shimoura, K. Ekuni, K. Sugimoto, N. Takahashi and T. Shimoda, Phys. Lett. **B 206** (1988) 592.
- [8] R. Anne *et. al.*, Phys. Lett. **B 250** (1990) 19; K. Riisager *et. al.*, Nucl. Phys. **A540** (1992) 365.
- [9] G. F. Bertsch, B. A. Brown and H. Sagawa, Phys. Rev. **C 39** (1989) 1154.
- [10] H. Sagawa, Phys. Lett. **B 286**, 7 (1992).
- [11] Z. Y. Zhu, W. Q. Shen, Y. H. Cai, and Y. G. Ma, Phys. Lett. **B 328**, 1 (1994).
- [12] T. Hoshino, H. Sagawa and A. Arima, Nucl. Phys. **A506** (1990) 271.

- [13] J.-F. Berger, J.-Dechargé and D. Gogny, Proceedings to the “Workshop on Nuclear Structure Models”, Oak Ridge, TN, March 16-25, 1992.
- [14] J. Dechargé and D. Gogny, Phys. Rev. **C 21** (1980), 1568.
- [15] P. Ring and P. Schuck, **The Nuclear Many-Body Problem** (New York: Springer-Verlag, 1980).
- [16] C. R. Chinn, J.-F. Berger, D. Gogny and M. S. Weiss, Phys. Rev. **C 45** (1992) 1700.
- [17] E. Arnold, J. Bonn, A. Klein, R. Neugart, M. Neuroth, E.W. Otten, P. Lievens, H. Reich, W. Widdra and ISOLDE Collaboration, Phys. Lett. **B 281**, 16 (1992).

FIGURES

FIG. 1. The Total Hartree-Fock-Bogolyubov energy as a function of the constraint variable, $\langle r^2 \rangle$ for ^{11}Li and ^9Li is shown. The ^9Li result is taken from a spherically symmetric HFB calculation.

FIG. 2. In the upper panel the separate *rms* radii for the proton and neutron distributions is plotted for the constrained HFB calculation as a function of the square root of the constraint variable, the *rms* radii of the total matter distribution. The lower panel plots in a similar fashion the BCS pairing energies for the neutron and proton sectors.

FIG. 3. The energies for some of the lowest single particle states are plotted for the protons and neutrons in the upper and lower panels, respectively, for the constrained HFB calculation as a function of $\langle r^2 \rangle$.

FIG. 4. The neutron radial densities for the unconstrained HFB calculation are shown as a function of r . The solid and short-dashed curves correspond to the calculated neutron densities of ^{11}Li and ^9Li , respectively. The long-dashed curve represents the neutron density for the ^9Li core projected from ^{11}Li . The lower panel is a logarithmic plot of the upper panel with the x-axis extended.

FIG. 5. The proton radial density profiles are shown as a function of r . The solid and short-dashed curves correspond to the unconstrained HFB calculation for ^{11}Li and ^9Li , respectively. The long-dashed curve is the result from the correlated GCM-type calculation. The lower panel is a logarithmic plot of the upper panel with the x-axis extended.

FIG. 6. The neutron radial density profiles are shown as a function of r . The solid and short-dashed curves correspond to the unconstrained HFB calculation of ^{11}Li and the projected ^9Li core of ^{11}Li , respectively. The long-dashed and dot-dashed curves are the result from the correlated GCM-type calculation for ^{11}Li and the projected ^9Li core of ^{11}Li , respectively. The shaded, fat long-dashed curve represents the difference between the long-dashed and the dot-dashed curves, thus corresponding to the two outer valence neutrons. The lower panel is a logarithmic plot of the upper panel with the x-axis extended.

FIG. 7. The neutron radial densities are shown for the constrained HFB calculation in a logarithmic plot as a function of r . The solid and long-dashed curves correspond to calculations using a 19 shell harmonic oscillator basis, where q is constrained to 3.4^2 and 4.0^2 fm^2 , respectively. The short-dashed and dot-dashed curves use three concentric eight shell harmonic oscillators as a basis, where q is constrained to 3.4^2 and 4.0^2 fm^2 , respectively.

FIG. 8. The collective neutron radial densities from the GCM-type calculation are shown, where the artificial tails of various listed categories were used for the densities calculated in the constrained HFB calculations.

Type of Calculation	$\langle r_{\text{total}} \rangle$ [fm]	$\langle r_{\text{proton}} \rangle$ [fm]	$\langle r_{\text{neutron}} \rangle$ [fm]
^{11}Li nucleus, unconstrained HFB	2.80	2.30	2.97
^{11}Li nucleus with correlations	3.42	2.31	3.75
^9Li core projected from ^{11}Li in unconstrained HFB	2.55	2.30	2.67
^9Li core projected from ^{11}Li with correlations	2.59	2.31	2.72
^9Li nucleus, unconstrained HFB	2.47	2.24	2.58
^{11}Li , experiment [7]	3.12(.16)	2.88(.11)	3.21(.17)
^9Li , experiment	2.32(.02)	2.18(.02)	2.39(.02)

Table I: The calculated *rms* radii for the neutron, proton and total matter distributions of ^{11}Li , ^9Li and the ^9Li core projected from ^{11}Li calculation are listed. The results from the pure mean field HFB and the correlated calculations are used.

With fitted tail	$\langle r_{\text{tot}} \rangle$	$\langle r_{\text{prot}} \rangle$	$\langle r_{\text{neut}} \rangle$
^{11}Li nucleus, HFB	2.80	2.30	2.96
^{11}Li w/correlations	3.42	2.31	3.75
^{11}Li Case a	2.88	2.31	3.07
^{11}Li Case b	2.84	2.31	3.02
^{11}Li Case c	2.85	2.31	3.03
^{11}Li Case d	2.86	2.31	3.04
^{11}Li Case e	2.87	2.31	3.05

Table II: The calculated *rms* radii in fm for the neutron, proton and total matter distributions of ^{11}Li including correlations are tabulated using various fitted asymptotic tails.

Type of Calculation	$\langle Q_{20}^{proton} \rangle$ [mB]	$\langle Q_{20}^{neutron} \rangle$ [mB]
^{11}Li unconstrained HFB	-31.20	-11.08
Correlated GCM ^{11}Li	-31.13	2.87
^9Li core projected from ^{11}Li unconstrained HFB	-31.20	-54.94
^9Li core projected from correlated GCM ^{11}Li	-31.13	-53.76
Free ^9Li , HFB, <i>DIS</i>	-43.46	-96.24
^{11}Li , experiment [17]	-31.2 (4.5)	
^9Li , experiment [17]	-27.4 (1.0)	

Table III: The calculated axial quadrupole moments in millibarns for the neutron, proton and total matter distributions of ^{11}Li , ^9Li and the ^9Li core projected from ^{11}Li calculation are listed. The results from the axial HFB and GCM calculations are used.

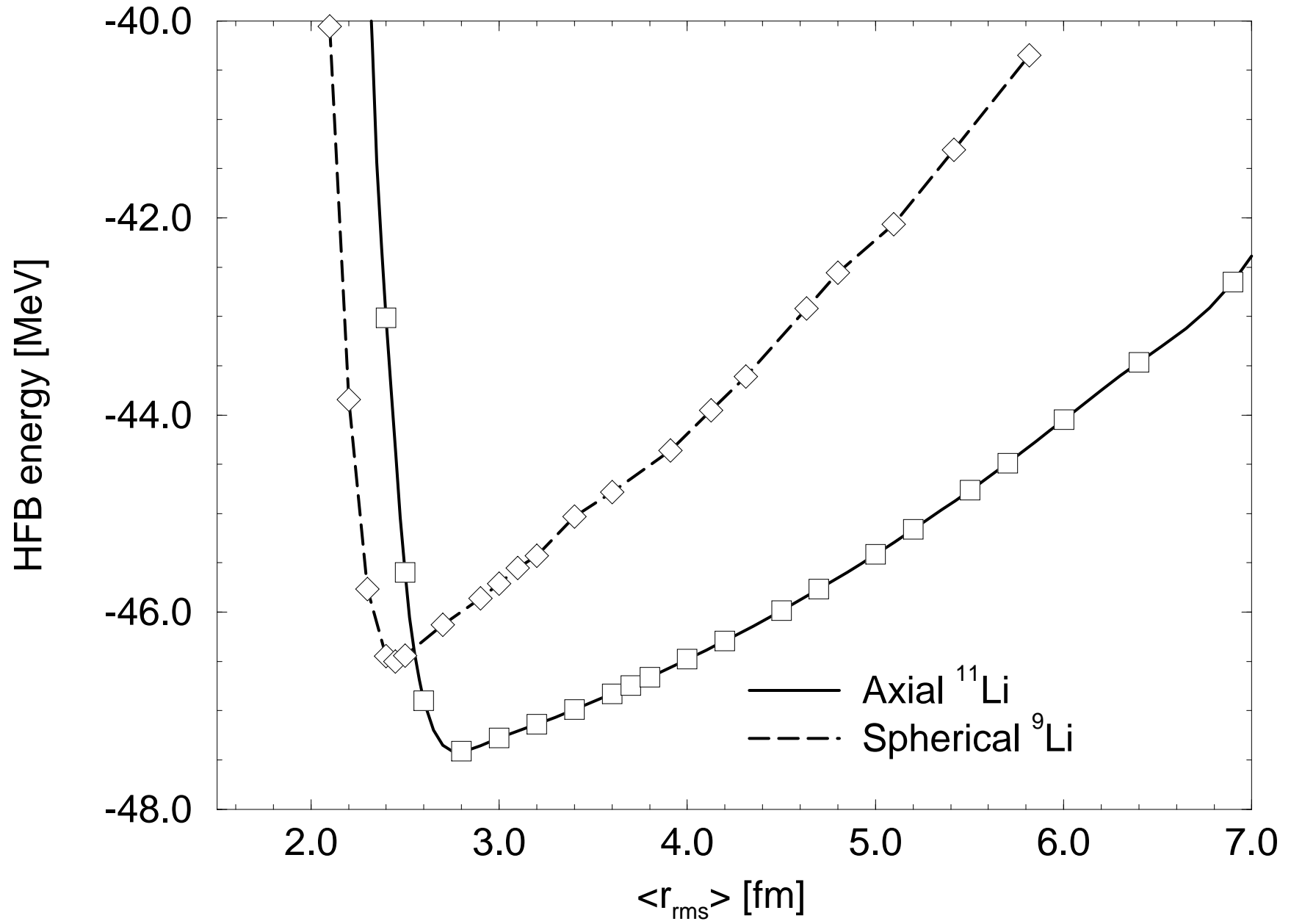
This figure "fig1-1.png" is available in "png" format from:

<http://arxiv.org/ps/nucl-th/9410033v1>

This figure "fig2-1.png" is available in "png" format from:

<http://arxiv.org/ps/nucl-th/9410033v1>

Figure 1



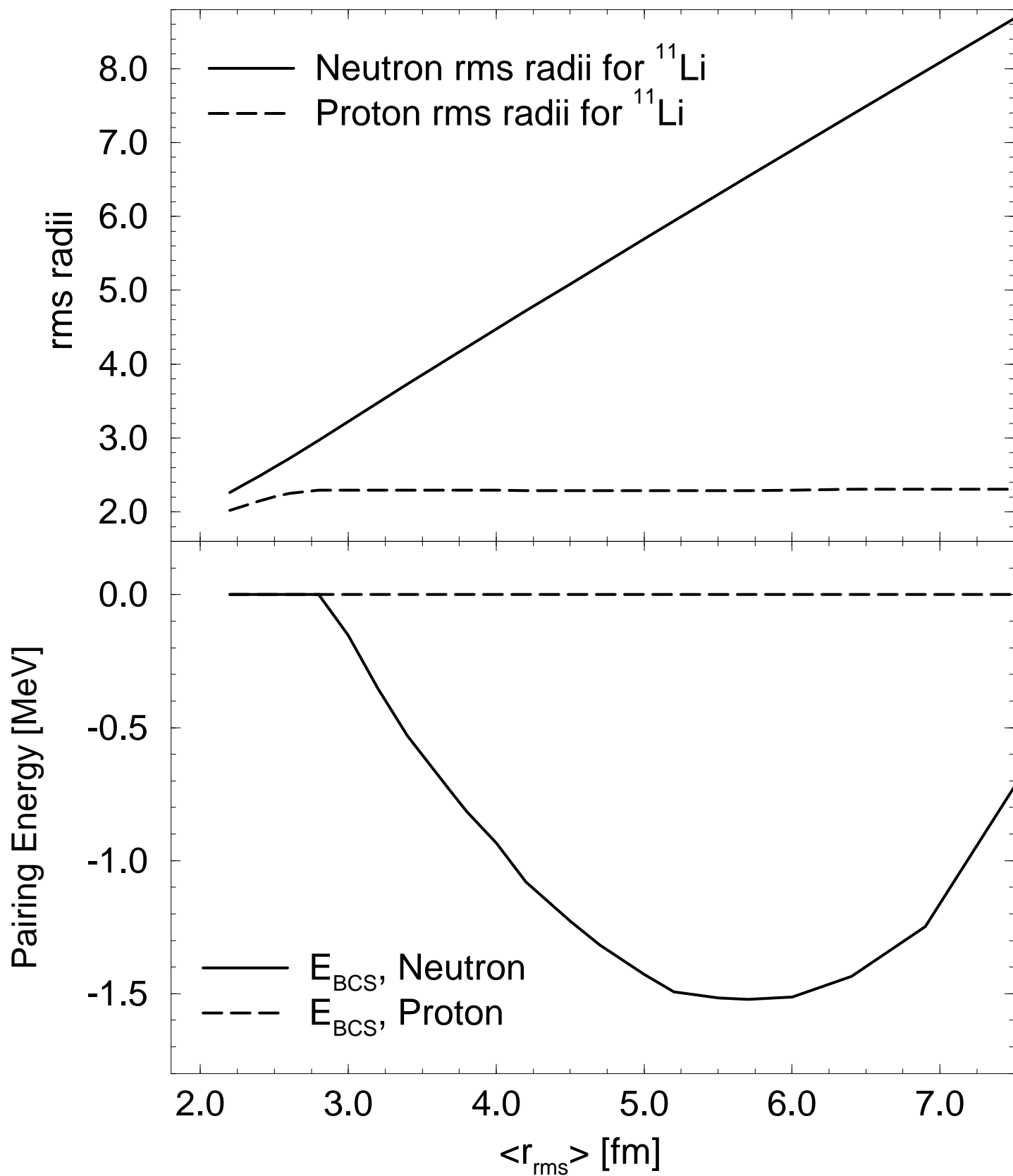
This figure "fig1-2.png" is available in "png" format from:

<http://arxiv.org/ps/nucl-th/9410033v1>

This figure "fig2-2.png" is available in "png" format from:

<http://arxiv.org/ps/nucl-th/9410033v1>

Figure 2



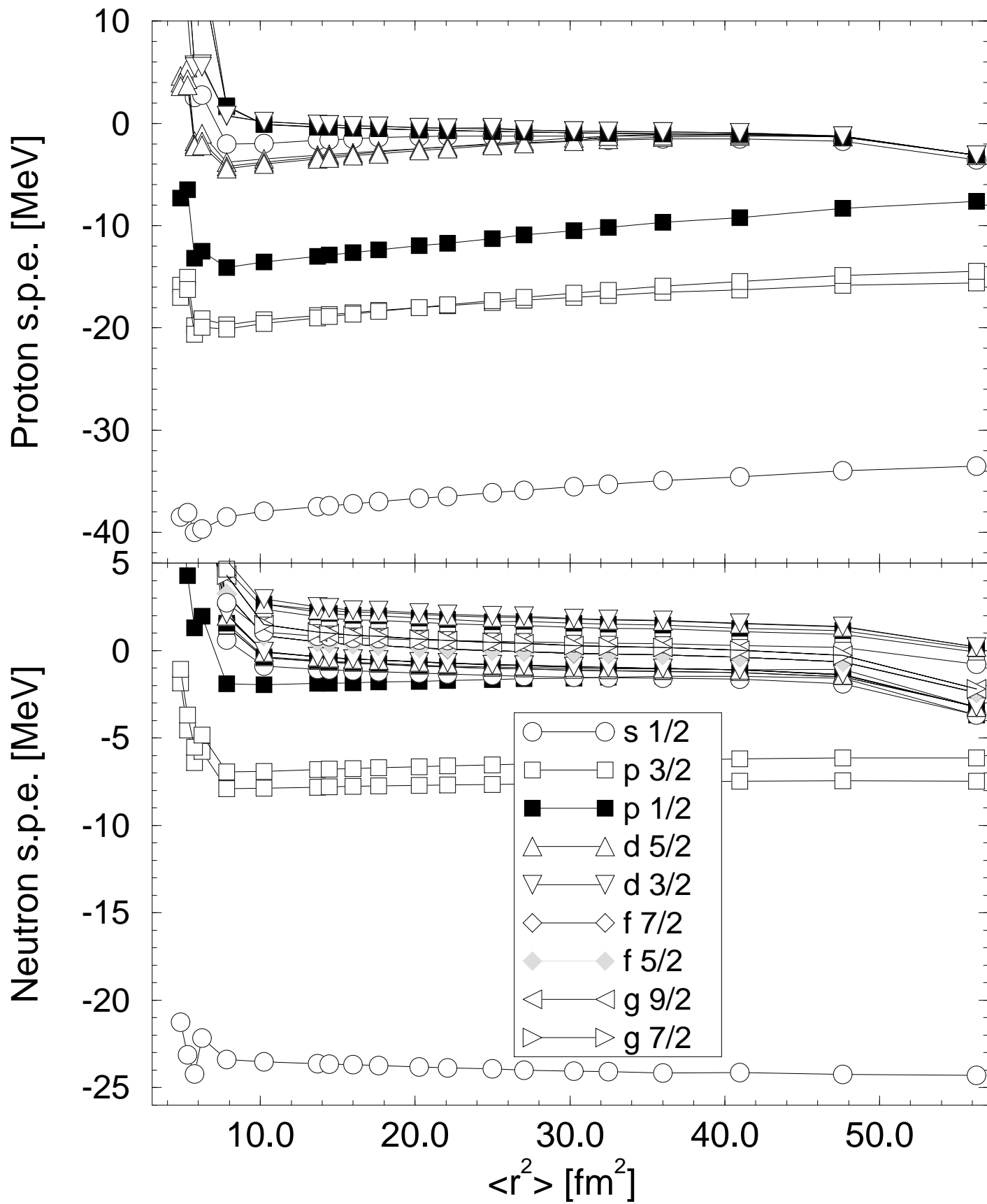
This figure "fig1-3.png" is available in "png" format from:

<http://arxiv.org/ps/nucl-th/9410033v1>

This figure "fig2-3.png" is available in "png" format from:

<http://arxiv.org/ps/nucl-th/9410033v1>

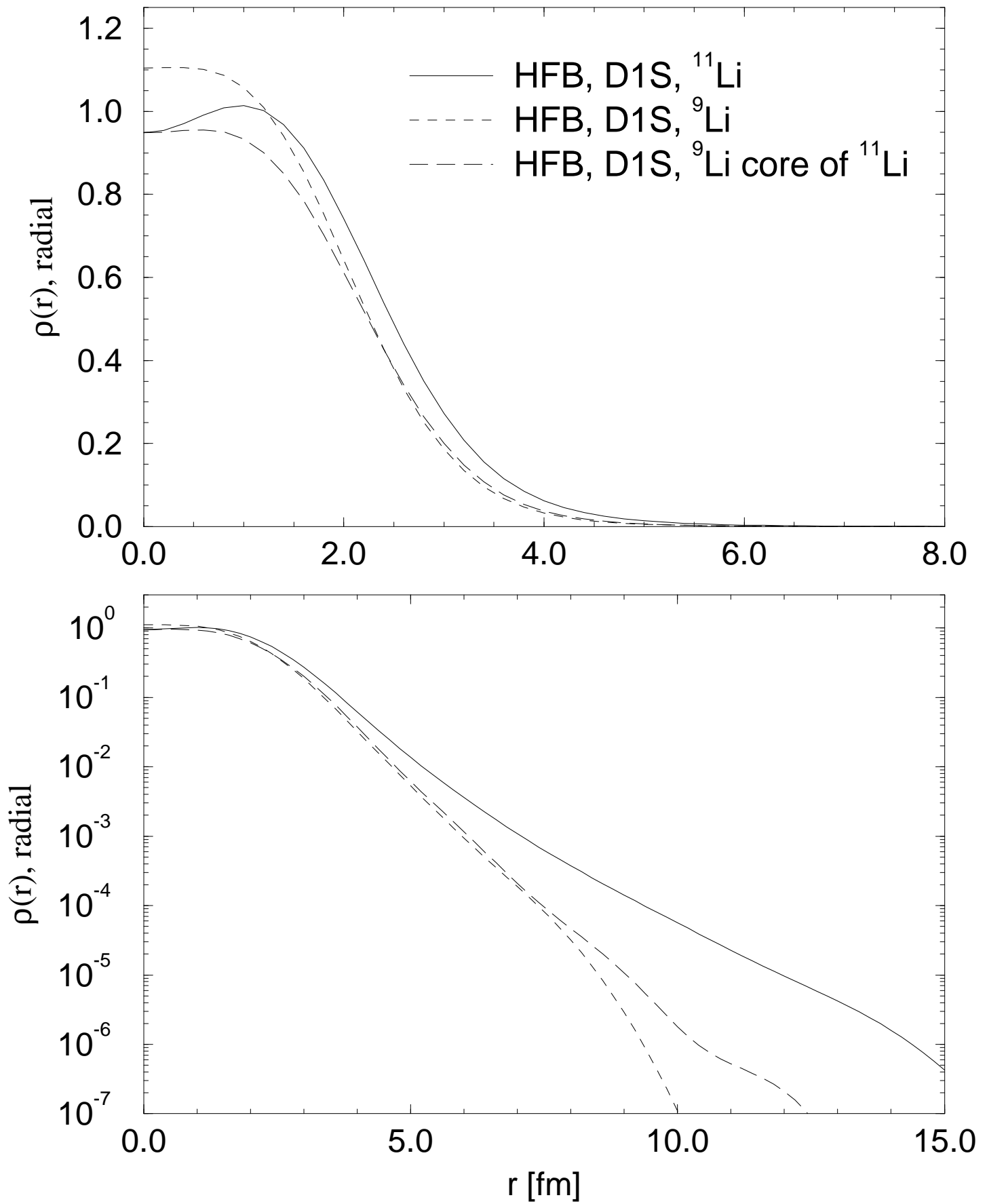
Figure 3



This figure "fig1-4.png" is available in "png" format from:

<http://arxiv.org/ps/nucl-th/9410033v1>

Figure 4



This figure "fig1-5.png" is available in "png" format from:

<http://arxiv.org/ps/nucl-th/9410033v1>

Figure 5

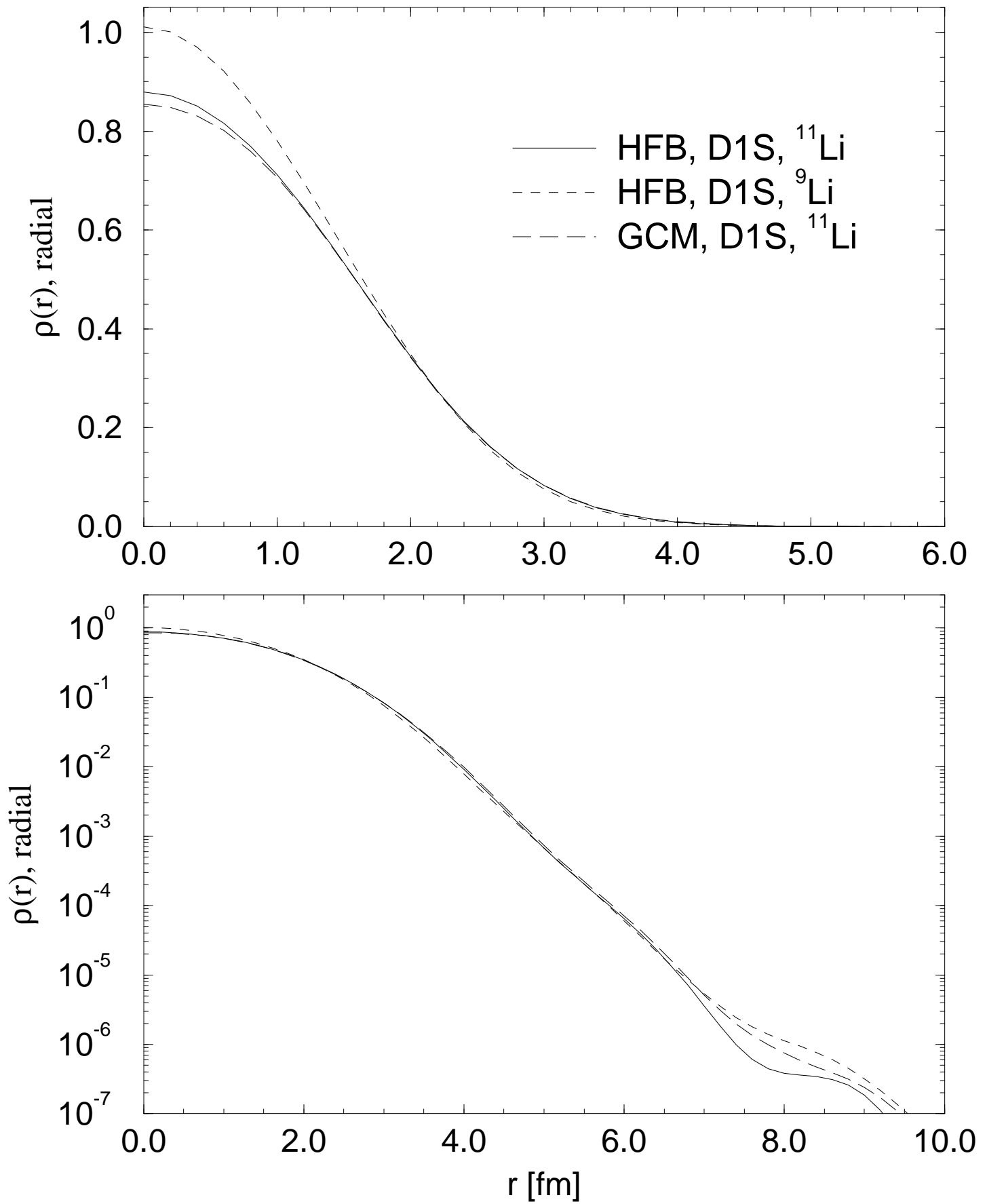


Figure 6

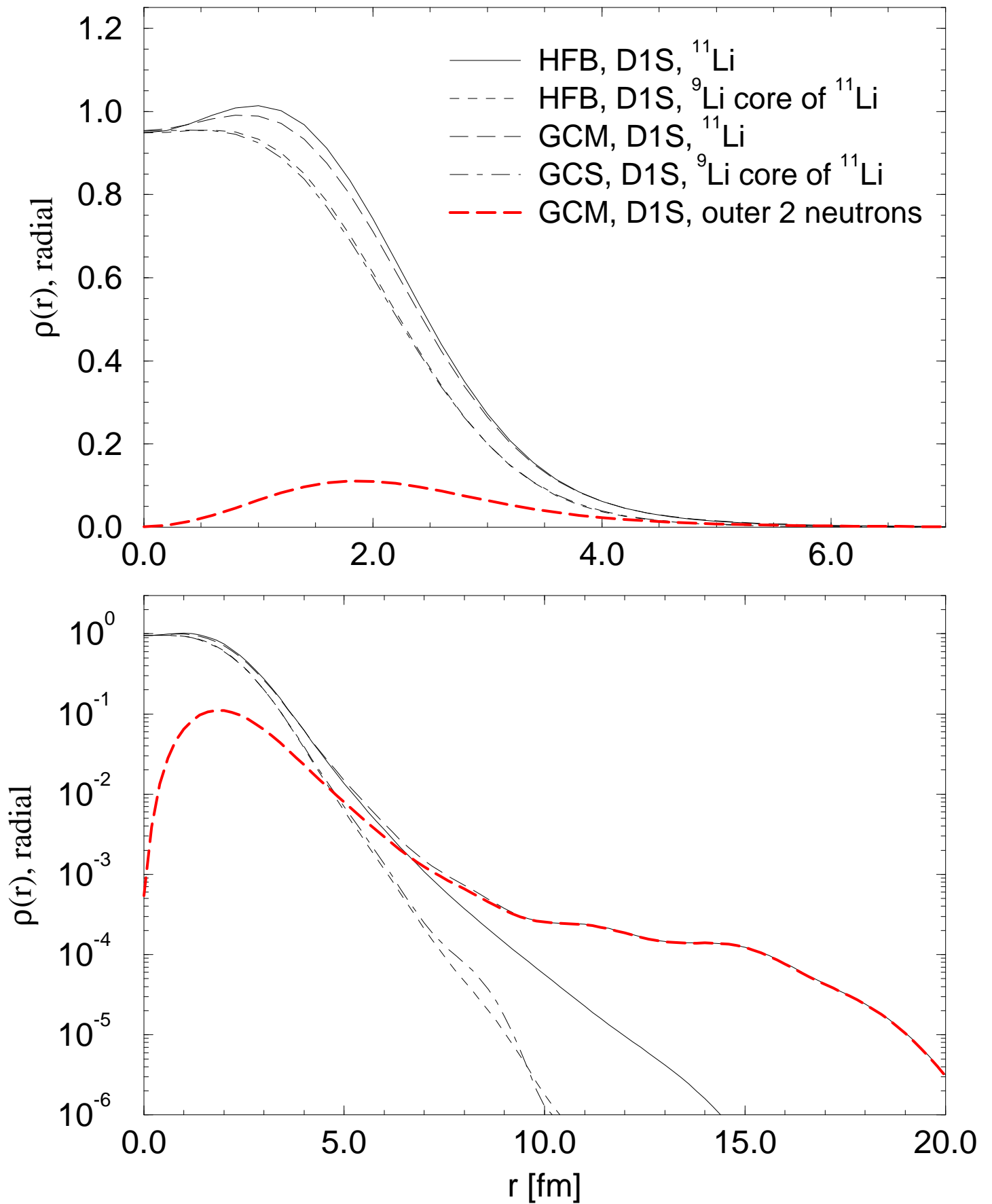


Figure 7

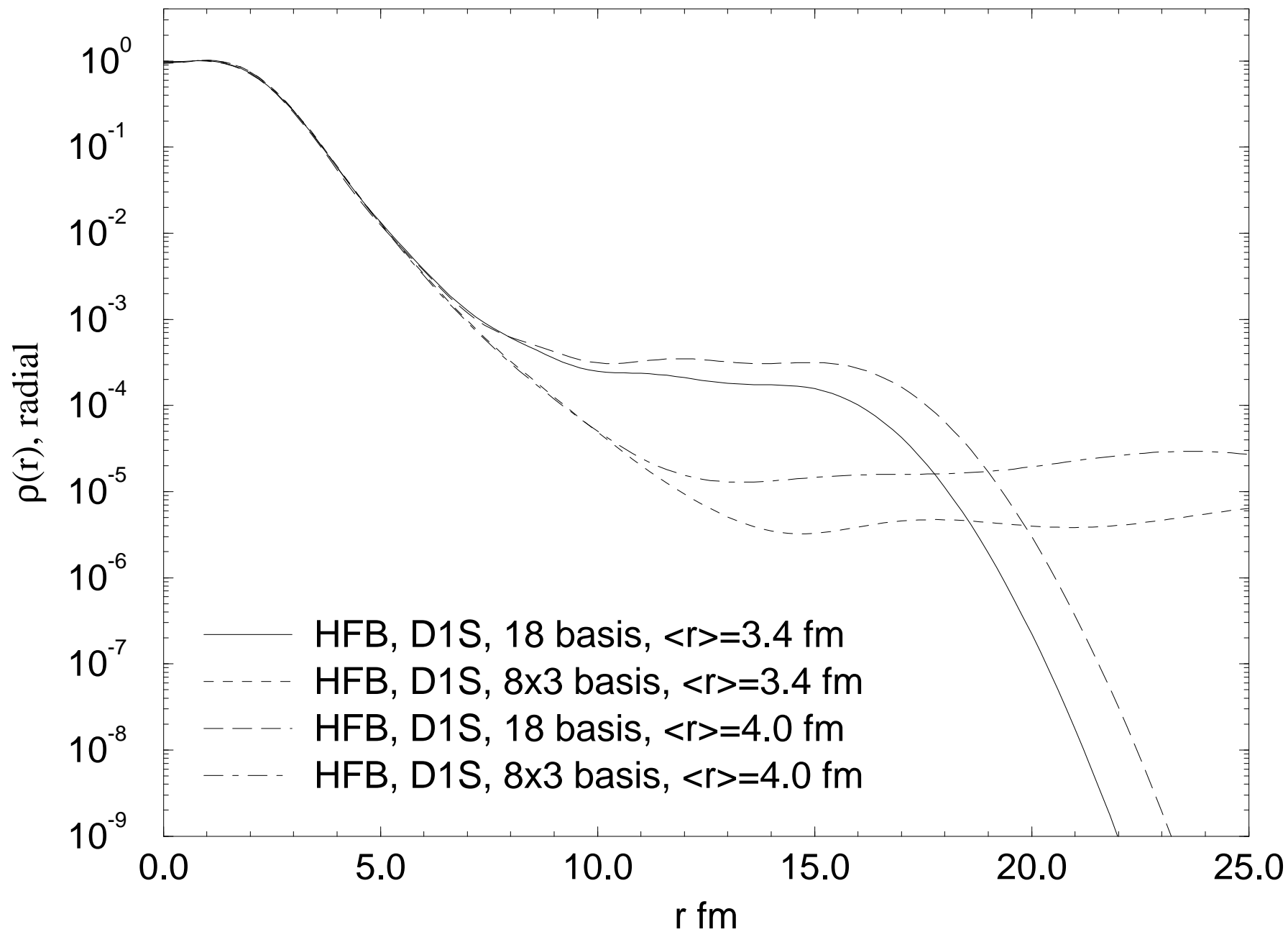


Figure 8

